Available online at www.sciencedirect.com
SCIENCE DIRECT®
Journal of Power Sources 133 (2004) 188–204
JOURNAL OF POWER SOURCES
www.elsevier.com/locate/jpowsour

System level lumped-parameter dynamic modeling of PEM fuel cell

X. Xue [a], J. Tang [a,*], A. Smirnova [b], R. England [b], Nigel Sammes [b]

[a] *Department of Mechanical Engineering, The University of Connecticut, 191 Auditorium Road, Unit 3139, Storrs, CT 06269, USA*
[b] *Connecticut Global Fuel Cell Center, University of Connecticut, 44 Weaver Road, Unit 5233, Storrs, CT 06269, USA*

Received 12 December 2003; accepted 31 December 2003

Abstract

The goal of this study is to develop a system-level dynamic model of a proton-exchange membrane (PEM) fuel cell that is capable of characterizing the mixed effects of temperature, gas flow, and capacitance, with particular emphasis focused on system transient behavior. The fuel cell system is divided into three control volumes and thus a lumped-parameter model for these sub-systems is established using a combination of intrinsic mechanistic relations and empirical modeling. The dynamic model is simulated using SIMULINK. The analysis illustrates the complicated dynamic interactions between various components and effects within a fuel cell system, and demonstrates the necessity of the proposed approach of separate control volumes. Numerical studies are correlated to a single-cell experimental investigation, and a protocol for parameter identification is explored to refine the model fidelity. The proposed fuel cell model can accurately predict the dynamic behavior and exhibits excellent agreement with experimental results. This model can be readily employed in the optimization and real-time control of PEM fuel cells installed in practical automotive or stationary applications.

Keywords: PEM fuel cell; System-level modeling; Lumped-parameter model; Transient dynamics; Control volume approach

1. Introduction

A proton-exchange membrane fuel cell (PEMFC) is an electrochemical device that converts the chemical energy of hydrogen and oxygen, with the aid of electro-catalysts, directly into electrical energy. After four decades of research and development, this device has reached the test and demonstration phase [1]. Typically, the analysis and design of PEMFCs are centered around the membrane–electrode assembly (MEA). The modeling of an MEA involves the characterization of physical environment of the electrochemical reaction, the transport phenomena of gas (hydrogen, oxygen, water vapor, etc.), water, proton and current, and the relationship between the fuel cell voltage, current, temperature, material (electrode, catalyst and membrane) properties and transport parameters. Traditional MEA modeling is mechanistic in essence [2–7]. Attempts have been made to investigate multi-species diffusion through the substrate and the diffusion layer of the electrode, the reaction kinetics in the active layer (catalyst), and proton and water transport through membrane. The resultant models are generally governed by a set of complex partial differential equations. While the mechanistic models are built upon the rigorous mathematical descriptions of fundamental physics, they normally have very complicated expressions and oftentimes certain key physical parameters are difficult to quantify, which may in turn reduce the modeling effectiveness. Empirical modeling, by mapping the fuel cell voltage as a function of various contributing variables [8–11], on the other hand, has certain advantages in some applications. Although this approach does not usually examine in depth the underlying electrochemical process, it utilizes the phenomenological description based on benchmark experimental study to reduce the model complexity as well as computational time. Typically, such empirical MEA sub-models are used in large fuel cell system-level models [12–15].

While MEA modeling constitutes the kernel of PEMFC study, the dynamic modeling and simulation at system level are even more complicated and involve fluid-structure–heat-electrochemistry coupled behavior. Amphlett et al. [12] proposed a fuel cell dynamic model which includes fuel cell body temperature variation effect but used steady-state flow rate governing equations. Pukrushpan et al. [13] developed a system-level model that includes compressor, supply and return manifolds, humidifier, and anode and cathode channels. Similar work was performed by Iqbal [14] who studied a hybrid energy system with an embedded fuel cell.

* Corresponding author. Tel.: +1-860-486-5911.
E-mail address: jtang@engr.uconn.edu (J. Tang).

0378-7753/$ – see front matter © 2004 Elsevier B.V. All rights reserved.
doi:10.1016/j.jpowsour.2003.12.064

Yerramalla et al. [15] considered the humidifier and stack pressure in the system level fuel cell modeling. It is worth noting that while the aforementioned studies have laid down a foundation for fuel cell system-level modeling, they had their respective emphases on certain aspects and have not addressed the *complete* dynamic effects within the system. A common simplification in references [13–15] is that the temperature transient behavior was neglected. On the other hand, it has been well recognized that temperature is a key parameter affecting the performance of the fuel cell. While low temperature of the cell could lead to flooding of the membrane, high temperature could cause a dry membrane, both of which could reduce the performance of the fuel cell in terms of heat and water management. Indeed, the fuel temperature and gas flow play key roles in fuel cell operation, and their dynamic effects should be simultaneously and accurately characterized in a fuel cell model in order for such a model to be effective within the entire operating range. It should be noted that some of the previous studies have not been completely correlated to experimental investigations.

It is the goal of this study to develop a system-level dynamic model of a PEMFC that incorporates the complicated temperature, gas flow and capacitance effects under operating conditions. The focus is on the dynamic and transient properties of the system. We will use the control volume approach [16] to develop a set of complete dynamic equations that govern the system dynamics. The fuel cell system is divided into three control volumes, the anode channel, the cathode channel, and the fuel cell body. For each control volume, the establishment of a lumped-parameter dynamic model is realized using a combination of intrinsic mechanistic relations and empirical modeling. The system-level model is simulated using SIMULINK, and a series of analyses are carried out. Numerical studies are then correlated to single-cell experimental investigations, and a protocol for parameter identification is explored to refine the model fidelity. This model is capable of characterizing the transient dynamic properties of a fuel cell system, and can be readily employed in the optimization and real-time control of PEMFCs installed in practical automotive or stationary applications.

2. Fuel cell modeling using control volume approach

In this study, we develop a mathematical model to investigate the mass and energy dynamic interactions as well as the electrochemical reaction within a PEMFC by using lumped parameters. As shown in Fig. 1, hydrogen enters the anode channel, part of which diffuses through the anode diffusion layer to the active catalyst layer, where the hydrogen dissociates into protons and electrons. The protons travel from the anode catalyst, through the membrane, to the cathode catalyst. In the meantime, oxygen enters the cathode channel, part of which diffuse through the cathode diffusion layer to the active catalyst, where the oxygen dissociates and combines with protons and electrons to form water, while heat and current are generated. The heat produced during the reduction reaction process will warm up the fuel cell body, which will affect the mass diffusion within the anode diffusion layer, cathode diffusion layer and membrane. Typically, the heat transfers to ambient and gas flow channels through convection and radiation. The resulting gas temperature variation will change the pressure and flow rate within the channels, which therefore affects the gas diffusion within the diffusion layers. All these dynamic interactions will have a direct effect on the fuel cell output voltage.

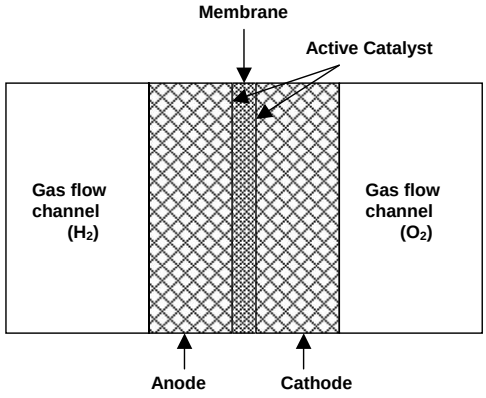

Fig. 1. Schematic illustration of a PEM fuel cell.

Throughout this paper, we assume an ideal gas mixture [19], which means that each mixture component behaves as an ideal gas as if it were alone. The momentum equation is not included, as we are concerned with macroscopic level dynamic properties. A no-slip condition at the fixed wall is assumed, and the viscous normal stresses at the inlet and outlet are neglected.

2.1. Modeling of mass and energy transfer using control volume approach

2.1.1. General governing equations

In this subsection, we present the basic governing equations for mass and energy interactions. The detailed description of the mathematical model for each control volume will be given in the subsequent subsections.

For an arbitrary control volume, the continuity equation in integral form is given as [16]

$$\frac{\partial}{\partial t}\iiint_{\text{C.V.}} \rho \,\mathrm{d}V + \oiint_{\text{C.S.}} \rho(\vec{V}\cdot\vec{n})\,\mathrm{d}A = 0 \tag{1}$$

and the energy equation in integral form is [16]

$$\frac{\partial}{\partial t}\iiint_{\text{C.V.}} \rho e_t \,\mathrm{d}V + \oiint_{\text{C.S.}} \rho h(\vec{V}\cdot\vec{n})\,\mathrm{d}A = \frac{\mathrm{d}Q}{\mathrm{d}t} + \frac{\mathrm{d}W}{\mathrm{d}t} \tag{2}$$

where ρ is the material density within the control volume, $\vec{V}$ the velocity vector of flow fluid, $\vec{n}$ the unit vector normal to the control surface toward the outside, e_t the specific

internal energy, h the specific enthalpy, Q the heat added to the control volume, and W the work done on the control volume. Note that typical gas flow velocity is low under fuel cell operating conditions. The kinetic and potential energy of the gases is thus neglected in the energy equation.

In a fuel cell system, there are complicated mass and energy interactions between the gas flow channels, cell body and MEA. In order to quantify such interactions, in this paper we define three control volumes, the anode channel, the cathode channel, and the body of the fuel cell. The anode channel control volume is the lumped volume from the anode inlet to the anode outlet. The cathode channel control volume is similarly defined at the cathode side. The MEA and all other metal structures involved in the fuel cell will form the fuel cell body control volume. When a fuel cell stack is considered, the anode channel, cathode channel and body control volumes will be the summation of corresponding control volumes of each single cell. The physical properties associated with the control volumes are assumed to be uniform. That is, in this study within the control volume we consider the average effect. In the subsequent subsections, we will use Eqs. (1) and (2) to derive detailed governing equations corresponding to the three control volumes. Since the characterization of water vapor is extremely complicated and involves phase change, such effects are not considered in the present study.

2.1.2. Anode and cathode channels

For the control volumes corresponding to the anode and cathode channels, the first term in Eq. (1) becomes the mass change rate of the respective gases. The second term in Eq. (1) is the mass flow rate through the surface of the control volumes. For an individual channel, three kinds of mass flow rate are involved, which correspond to, the gas entering the flow channel from the inlet, the gas leaving the channel from the outlet, and the gas diffusion through the anode/cathode diffusion layers, respectively, as described in Fig. 1

$$\oiint_{\text{C.S.}} \rho(\vec{V}\cdot\vec{n})\,\mathrm{d}A = \iint_{\text{inlet}} \rho(\vec{V}\cdot\vec{n})\,\mathrm{d}A + \iint_{\text{outlet}} \rho(\vec{V}\cdot\vec{n})\,\mathrm{d}A + \iint_{\text{electrode}} \rho(\vec{V}\cdot\vec{n})\,\mathrm{d}A \tag{3}$$

The velocity profiles are required for the calculation of Eq. (3). In general, the instant velocity profile can be obtained by solving the momentum equation simultaneously. This paper deals with the macroscopic level dynamic behavior of the fuel cell, and the mass flow through the inlet/outlet control surfaces will be simplified as the traditional nozzle flow rate equation [13]

$$\iint \rho(\vec{V}\cdot\vec{n})\,\mathrm{d}A = k(\Delta p) \tag{4}$$

where Δp denotes the pressure difference, and k the mass flow rate coefficient which in turn depends upon temperature and pressure difference.

The third term on the right-hand side of Eq. (3) involves a complicated process. Hydrogen diffuses through the porous gas-diffusion anode to anode catalyst, where the electrochemical reaction takes place to form a proton and an electron; oxygen diffuses through the porous gas-diffusion cathode to cathode catalyst, where the reduction reaction takes place to form water and heat. During the electrochemical/reduction reaction, current is generated. Although such processes at the catalyst layer are complicated and still subject to intensive study, it complies with the macroscopic level mass and species conservation law, i.e., the consumed hydrogen and oxygen have a definitive relationship with the current generated [13]

$$\iint_{\text{electrode}} \rho(\vec{V}\cdot\vec{n})\,\mathrm{d}A = N\frac{i}{nF}M \tag{5}$$

where i denotes the current, N the number of cells in a stack, and F, M and n are Faraday constant, gas mole mass and constant corresponding to different gas species, respectively.

The general energy equation (Eq. (2)) can be applied to the anode and cathode channels in a similar manner. The first term on the left-hand side of Eq. (2) represents the internal energy change rate within the control volume. The second term in Eq. (2) is the heat transfer rate due to the mass transport through the control surface. Such mass transport involves the hydrogen in the anode channel that diffuses through the porous anode diffusion layer to the cell body and the oxygen in the cathode channel that diffuses through the porous cathode diffusion layer to the cell body. On the right-hand side of Eq. (2), the first term ($\mathrm{d}Q/\mathrm{d}t$) represents the rate of heat added to the control volume, which is generally caused by convection heat transfer or possible radiation between the cell body and the channels and between the cell body and the surrounding ambient. As the temperature of a PEMFC body is relatively moderate, the radiation effect can neglected. Newton's cooling law governs the convection heat transfer mechanism

$$\frac{\mathrm{d}Q}{\mathrm{d}t} = h_{\text{conv}}A_{\text{conv}}\,\Delta T \tag{6}$$

where h_{conv} is the convection heat transfer coefficient, A_{conv} the convection surface area, and ΔT denotes the temperature difference between the cell body and the channels/ambient. In this paper, the viscous normal stresses at the inlet, outlet and electrode interface of mass diffusion are neglected, and the work done on the control volume ($\mathrm{d}W/\mathrm{d}t$) disappears.

2.1.3. Cell body

It is well known that most parts of the cell body are composed of metal structures. The continuity equation (Eq. (1)) for the cell body control volume is only concerned with the species' conservation of electrochemical/reduction re-

action. That is, water is formed through the electrochemical/reduction reaction by consuming hydrogen and oxygen

$$\iint_{\text{electrode,an}} \rho_{H_2}(\vec{V}\cdot\vec{n})\,dA + \iint_{\text{electrode,ca}} \rho_{O_2}(\vec{V}\cdot\vec{n})\,dA = \dot{m}_{H_2O} \tag{7}$$

Hereafter, the variable m represents the mass, and the subscript designates specific species.

The energy equation (Eq. (2)) for the cell body control volume is now considered. The first term on the left-hand side is the cell body internal energy accumulation rate. The second term is the heat transfer to the cell body via mass transport. As discussed in the Section 2.1.2, such mass transport includes the diffusion of gases through the electrodes and the water produced by the electrochemical/reduction reaction that flows out from the cell body. There are several heat transfer effects involved in the term dQ/dt, which include the heat added to the cell body through the electrochemical/reduction reaction as well as the heat transferred to the ambient and the channels via convection

$$\frac{dQ}{dt} = \dot{Q}_{\text{conv,an}} + \dot{Q}_{\text{conv,ca}} + \dot{Q}_{\text{conv,amb}} + \Delta H_{R,T} \iint_{\text{eletrode}} \rho_{H_2}(\vec{V}\cdot\vec{n})\,dA \tag{8}$$

where, specifically, $Q_{\text{conv,an}}$ is the heat convection between the cell body and the anode channel, $Q_{\text{conv,ca}}$ the heat convection between the cell body and the cathode channel, $Q_{\text{conv,amb}}$ the heat convection between the cell body and the ambient, and $\Delta H_{R,T}$ the lower heating value of the fuel. All the heat convection terms here are assumed to comply with Newton's cooling law as shown in Eq. (6).For the cell body, the term dW/dt represents the electric power converted from electrochemical/reduction reaction, i.e.

$$\frac{dW}{dt} = -NV_{\text{cell}}i \tag{9}$$

where V_{cell} denotes the cell voltage that will be discussed in detail in Section 2.2.

2.1.4. Dynamic equations of three control volumes

Based upon the above discussions, we derive detailed lumped-parameter dynamic equations governing all three control volumes. Here we assume uniform thermo-physical properties throughout the procedure.

For the anode channel, the hydrogen mass change rate is such that

$$\frac{\partial}{\partial t}\iiint_{\text{C.V.}} \rho_{H_2}\,dV = \frac{dm_{H_2}}{dt} \tag{10a}$$

and the hydrogen mass transport rate through the anode channel control surface is given as

$$-\oiint_{\text{C.S.}} \rho_{H_2}(\vec{V}\cdot\vec{n})\,dA = k_{\text{up,an}}(p_{\text{s,an}} - p_{\text{an}}) - k_{\text{down,an}}(p_{\text{an}} - p_{\text{atm}}) - N\frac{i}{2F}M_{H_2} \tag{10b}$$

where $k_{\text{up,an}}$ and $k_{\text{up,an}}$ are inlet and outlet mass flow rate coefficients, and $p_{\text{s,an}}$, p_{an} and p_{atm} represent, respectively, the hydrogen source pressure, the pressure within the anode control volume and ambient pressure. The internal energy change rate of hydrogen within the anode channel control volume is given as

$$\frac{\partial}{\partial t}\iiint_{\text{C.V.}} \rho_{H_2} e_t\,dV = \frac{d(m_{H_2}c_{v,H_2}T_{\text{an}})}{dt} \tag{10c}$$

where c_{v,H_2} is the specific heat of hydrogen with constant volume, and T_{an} the hydrogen temperature within the anode channel control volume. The heat transfer to the anode channel control volume through the hydrogen mass transfer across the control surface, which includes inlet, outlet and electrode diffusion layer, is given as

$$-\oiint_{\text{C.S.}} \rho_{H_2}h_{H_2}(\vec{V}\cdot\vec{n})\,dA = k_{\text{up,an}}(p_{\text{s,an}} - p_{\text{an}})c_{p,H_2}(T_{\text{an,in}} - T_{\text{o}}) - k_{\text{down,an}}(p_{\text{an}} - p_{\text{atm}})c_{p,H_2}(T_{\text{an}} - T_{\text{o}}) - N\frac{i}{2F}M_{H_2}c_{p,H_2}(T_{\text{an}} - T_{\text{o}}) \tag{10d}$$

where $T_{\text{an,in}}$ and T_{o} represent the flow-in hydrogen temperature and the reference temperature, respectively. The convection heat transfer from the cell body to the anode channel is described as

$$\frac{dQ}{dt} = k_{\text{conv,an}}(T_{\text{body}} - T_{\text{an}}) \tag{10e}$$

where $k_{\text{conv,an}} = h_{\text{conv,an}}A_{\text{conv,an}}$, $h_{\text{conv,an}}$ is the heat convection coefficient, and $A_{\text{conv,an}}$ the surface area of heat convection.

We can derive similar relations for the cathode channel. The following equations are parallel to those given in Eqs. (10a)–(10e), and the relevant subscripts are replaced by "ca" (cathode) and "O_2" (oxygen)

$$\frac{\partial}{\partial t}\iiint_{\text{C.V.}} \rho_{O_2}\,dV = \frac{dm_{O_2}}{dt} \tag{11a}$$

$$-\oiint_{\text{C.S.}} \rho_{O_2}(\vec{V}\cdot\vec{n})\,dA = k_{\text{up,ca}}(p_{\text{s,ca}} - p_{\text{ca}}) - k_{\text{down,ca}}(p_{\text{ca}} - p_{\text{atm}}) - N\frac{i}{4F}M_{O_2} \tag{11b}$$

$$\frac{\partial}{\partial t}\iiint_{\text{C.V.}} \rho_{O_2} e_t\,dV = \frac{d(m_{O_2}c_{v,O_2}T_{\text{ca}})}{dt} \tag{11c}$$

$$-\oiint_{\text{C.S.}} \rho_{O_2} h_{O_2} (\vec{V}\cdot\vec{n})\,dA = k_{up,ca}(p_{s,ca}-p_{ca})c_{p,O_2}(T_{ca,in}-T_o) - k_{down,ca}(p_{ca}-p_{atm})c_{p,O_2}(T_{ca}-T_o) - N\frac{i}{4F}M_{O_2}c_{p,O_2}(T_{ca}-T_o) \quad (11d)$$

$$\frac{dQ}{dt} = k_{conv,ca}(T_{body}-T_{ca}) \quad (11e)$$

Finally we consider the cell body. Since most parts of the body are composed of metal structures and MEA and gas diffusion and water produced have little effect on the total mass change of cell body, we thus have

$$\frac{\partial}{\partial t}\iiint_{\text{C.V.}} \rho_{body}\,dV = 0 \quad (12a)$$

The mass transport rate through the cell body control surface (MEA) is given as

$$-\oiint_{\text{C.S.}} \rho_{body}(\vec{V}\cdot\vec{n})\,dA = N\frac{i}{2F}M_{H_2} + N\frac{i}{4F}M_{O_2} - \dot{m}_{H_2O} \quad (12b)$$

Note the above equation includes the gas diffusion through the electrodes and water formed by electrochemical/reduction reactions. The internal energy change rate of cell body is such that

$$\frac{\partial}{\partial t}\iiint_{\text{C.V.}} \rho_{body} e_t\,dV = m_{body}c_{p,body}\frac{dT_{body}}{dt} \quad (12c)$$

where $c_{p,body}$ is the average specific heat of the cell body. The heat added to and the work done on the cell body control volume can be characterized as

$$\frac{dQ}{dt}+\frac{dW}{dt} = k_{conv,an}(T_{an}-T_{body}) + k_{conv,ca}(T_{ca}-T_{body}) + k_{conv,amb}(T_{amb}-T_{body}) + \Delta H_{R,T}N\frac{i}{2F}M_{H_2} - NV_{cell}i \quad (12d)$$

Such effects include the convection heat transfer from the surrounding structures (the first three terms at right-hand side), heat produced by the electrochemical/reduction reaction (the fourth term on the right-hand side), and converted electric power (the last term).

2.2. Electrochemical modeling

In previous studies, empirical modeling has been developed for the MEA, which is built upon a phenomenological relationship between the fuel cell voltage and various contributing variables [8,9]. This approach has been employed in various system-level fuel cell modeling [12–15]. Typically, the cell voltage is assumed to depend upon state variables including the partial pressure of hydrogen and oxygen, the temperature of the cell body, and load current, etc.

$$V_{cell} = f(P_{H_2}, P_{O_2}, T_{body}, i, \alpha) \quad (13)$$

where P_{H_2} is the hydrogen partial pressure, P_{O_2} the oxygen partial pressure, T_s the body temperature, i the load current, and α represents other possibly related parameters. In this study, we use the same approach to perform the electrochemical modeling, which is based upon a curve-fitting method [9]. It is worth noting that, in classical empirical MEA modeling [9–11,17], the effective surface partial pressures are used in Eq. (13). In this study, in order to simplify the empirical MEA modeling for large fuel cell system, we use the hydrogen/oxygen partial pressures within the corresponding channels to obtain the empirical MEA model. While such direct utilization of hydrogen/oxygen partial pressures within the channels could lead to error in thermodynamic potential, such error can readily be compensated for in the activation overvoltage calculation. A detailed comparison will be provided in Section 3.2.

Generally, fuel cell voltage is the summation of three effects, the thermodynamic potential E_{Nernst}, the activation overvoltage η_{act} resultant from anode overvoltage and cathode overvoltage, and the ohmic overvoltage η_{ohmic}. For hydrogen/oxygen fuel cell, the thermodynamic potential is [19]

$$E_{Nernst} = 1.229 - (8.5\times10^{-4})(T_{body}-298.15) + (4.308\times10^{-5})T_{body}[\ln(P_{H_2}) + 0.5\ln(P_{O_2})] \quad (14)$$

Here, we will use the channel hydrogen/oxygen partial pressure instead of the effective partial pressure used in [9]. The activation overvoltage can be written as

$$\eta_{act} = \xi_1 + \xi_2 T_{body} + \xi_3 T_{body}\ln(i) + \xi_4 T_{body}\ln(c_{O_2}) \quad (15)$$

The parameters ξ_i in Eq. (15) can be obtained from experimental data using a linear regression technique. While various empirical expressions for activation overvoltage exist, one can always use curve fitting to obtain a proper mathematical model [9,14,18]. The ohmic overvoltage is given as

$$\eta_{ohmic} = -iR^{internal} \quad (16)$$

where $R^{internal}$ is the lumped resistance caused by resistances in electron flow, proton flow and other contact resistances. The empirical equation for internal resistance uses the format as follow [9]

$$R^{internal} = \xi_5 + \xi_6 T_{body} + \xi_7 i \quad (17)$$

where the coefficients ξ_i will also be solved using a linear regression method.It should be noted that Eqs. (15) and (17) apply only to the steady-state case. In order to capture the transient dynamic behavior, in this study we incorporate the effect of double charged layers [12,16] by defining the activation resistance as

$$R_a = -\frac{\eta_{act}}{i} \quad (18)$$

The dynamic activation overvoltage is then governed by

$$\frac{dv_{act}}{dt} = \frac{i}{C} - \frac{v_{act}}{R_a C} \quad (19)$$

which yields the total cell voltage as

$$V_{\text{cell}} = E_{\text{Nernst}} + v_{\text{act}} + \eta_{\text{ohmic}} \quad (20)$$

The modeling of the overall fuel cell system is then completed.

3. Benchmark simulation and experimental correlation

Outlined in Section 2 are the main dynamic equations of a fuel cell system. In this section, we present a series of analysis results to verify the developed model and to study the complicated dynamic interactions between various components and effects. The mathematical model is implemented using MATLAB/SIMULINK, as shown in Fig. 2.

3.1. Benchmark study and analysis

We first compare the newly developed model with the benchmark work performed by Amphlett et al. [12], and demonstrate the improvement in the proposed work. In that study, while the temperature transient behavior of stack/cell is considered, the modeling of gas flows is based on steady-state equations. In fact, the model developed in [12] can be considered as a special case of the dynamic model we have developed in this research. This can be illustrated by the following analysis.

Consider the anode channel control volume continuity equations given as (1), (10a) and (10b). If we assume steady-state flow, we have

$$k_{\text{up,an}}(p_{\text{s}} - p_{\text{an}}) - k_{\text{down,an}}(p_{\text{an}} - p_{\text{atm}}) = N\frac{i}{2F}M_{\text{H}_2} \quad (21)$$

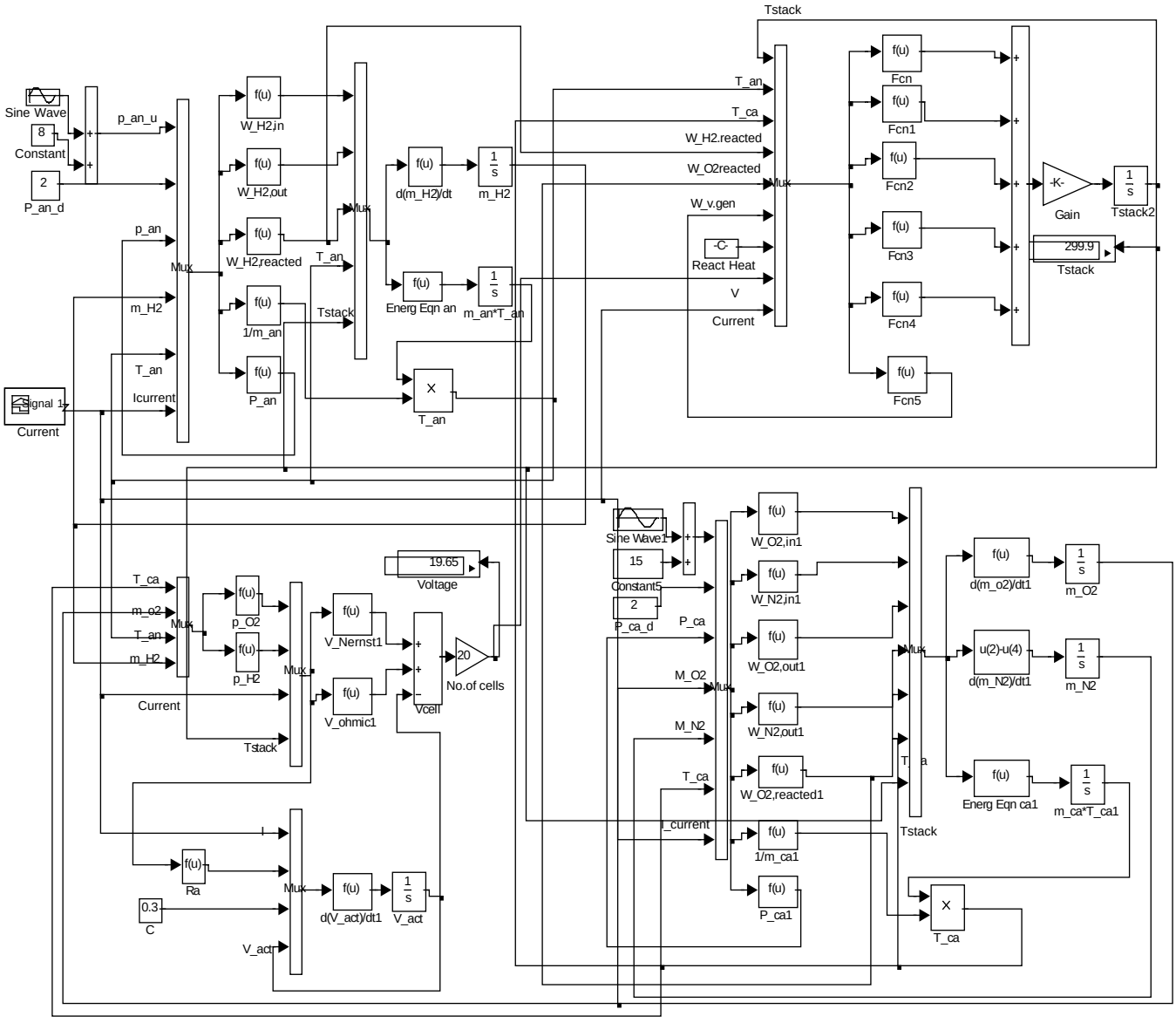

Fig. 2. SIMULINK block diagram of the mathematical model.

In virtue of Eqs. (4) and (5), one can get

$$\dot{m}_{H_2,an,in} = k_{up,an}(p_s - p_{an}) \tag{22a}$$

$$\dot{m}_{H_2,an,out} = k_{down,an}(p_{an} - p_{atm}) \tag{22b}$$

$$\dot{m}_{H_2,cons} = N\frac{i}{2F}M_{H_2} \tag{22c}$$

Substituting Eqs. (22a)–(22c) into (21), we can obtain exactly the analytical flow rate relation given in [10]. Similar assumption can be applied to cathode channel control volume, and we can again get the same conclusion. Therefore, the flow rate equations presented in [12] are the steady-state special case of our model.

We then compare the energy equations of our model with those given in [12]. In that study, Amphlett et al. defined four energy terms, the theoretical energy produced by electrochemical reaction (q_{theo}), the electrical energy output (q_{elec}), the heat loss rate from stack surface through heat convection (q_{loss}), and the sensible heat terms for each of the fuel cell streams (anode, cathode, and water) (q_{sens}). Here, we again use anode channel for illustration. Based upon the notations used in this research, the aforementioned energy terms satisfy the following relations

$$\dot{q}_{sens,a} = \oiint_{C.S.} \rho_{H_2} h_{H_2} (\vec{V}\cdot\vec{n})\,dA \tag{23a}$$

$$\dot{q}_{loss,a} = k_{conv,an}(T_{body} - T_{an}) \tag{23b}$$

$$\frac{d(m_{H_2} c_{v,H_2} T_{an})}{dt} = -\dot{q}_{sens,an} + \dot{q}_{loss,an} \tag{23c}$$

Table 1
Parameters used in the comparison simulation [12]

Parameter	Value	Parameter	Value
$N_{H_2,an,in}$ (mol/s)	0.0078	$N_{H_2,an,out}$ (mol/s)	0.004
$T_{an,in}$ (°C)	23.5	$T_{an,out}$ (°C)	25.3
$N_{O_2,an,in}$ (mol/s)	0.004	$N_{O_2,an,out}$ (mol/s)	0.002
$T_{ca,in}$ (°C)	23.5	$T_{ca,out}$ (°C)	38.8
$(hA)_{an}$ (W/K)	2	$(hA)_{ca}$ (W/K)	10
$(hA)_{H_2O}$ (W/K)	50	$(hA)_{stack}$ (W/K)	17
MC (kJ/K)	35		

If we assume the steady-state operating condition, the left-hand side of Eq. (23c) vanishes, which yields

$$\dot{q}_{sens,an} = \dot{q}_{loss,an} \tag{23d}$$

The above relation is exactly the same as that shown in [12]. Similar results can be obtained for the cathode control volume and water flow stream. Clearly, the energy equations related to gases and water streams presented in [12] are also the steady-state special case of our model. We can then conclude that the model developed in [12] is generally a special case of the present work. The above analytical demonstration shows that the newly developed model will yield the same simulation result under certain steady-state assumptions.

One thing worth noting is that in dealing with the sensible heat term, Amphlett et al. did not take into consideration the hydrogen diffusion through the electrode [12]. Such effect is included in the current model and can be illustrated by using the data provided in [12] (shown in Table 1). The load current changes from 0 to 20 A, and as a result the output voltage changes from 38 to 28.6 V

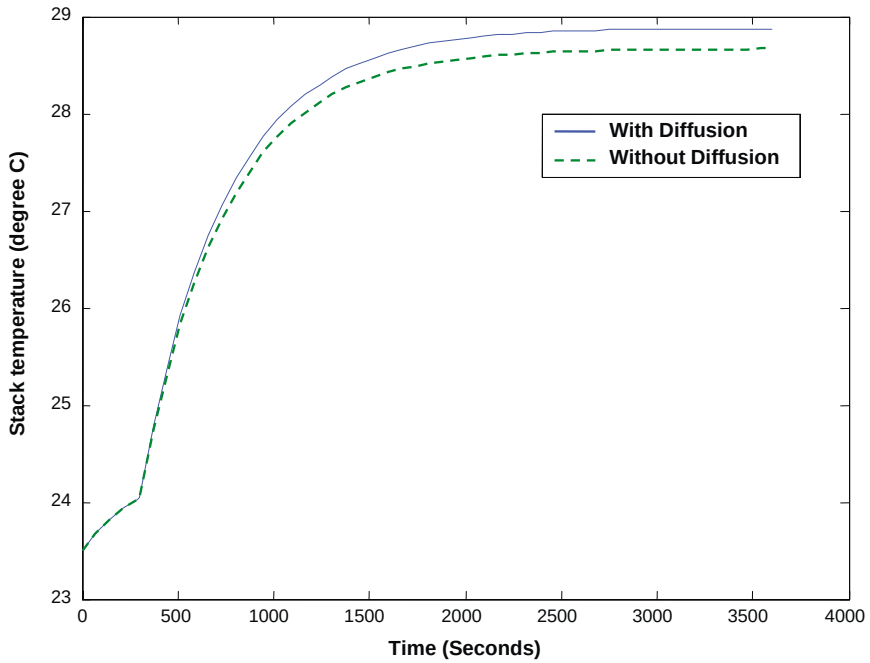

Fig. 3. Effect of diffusion on transient stack temperature.

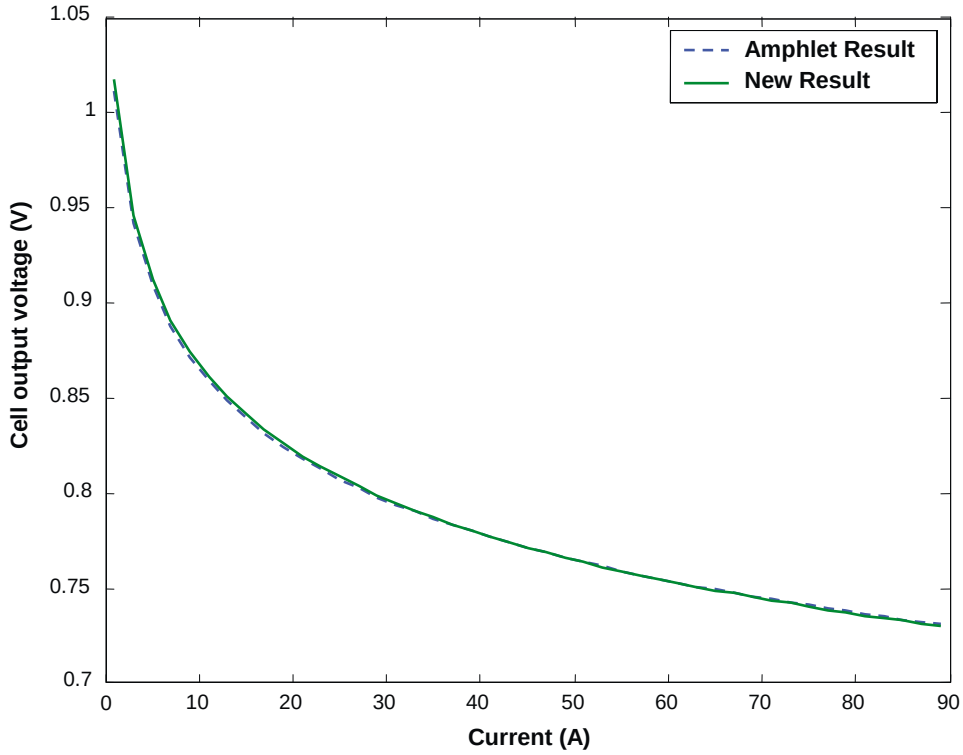

Fig. 4. Empirical model comparison.

[12]. We study the stack temperature history, and the simulation result is shown in Fig. 3. Clearly, the gas diffusion will affect the stack temperature. One can further envision that for a larger current situation, this effect will become even more significant, as the consumed gases will further increase.

3.2. Modification of empirical MEA model development

Amphlett et al. [11] developed an empirical MEA model predicting the fuel cell output voltage, activation overvoltage and internal resistance based on experimental results. Such approach has been adopted in many system-level PEMFC

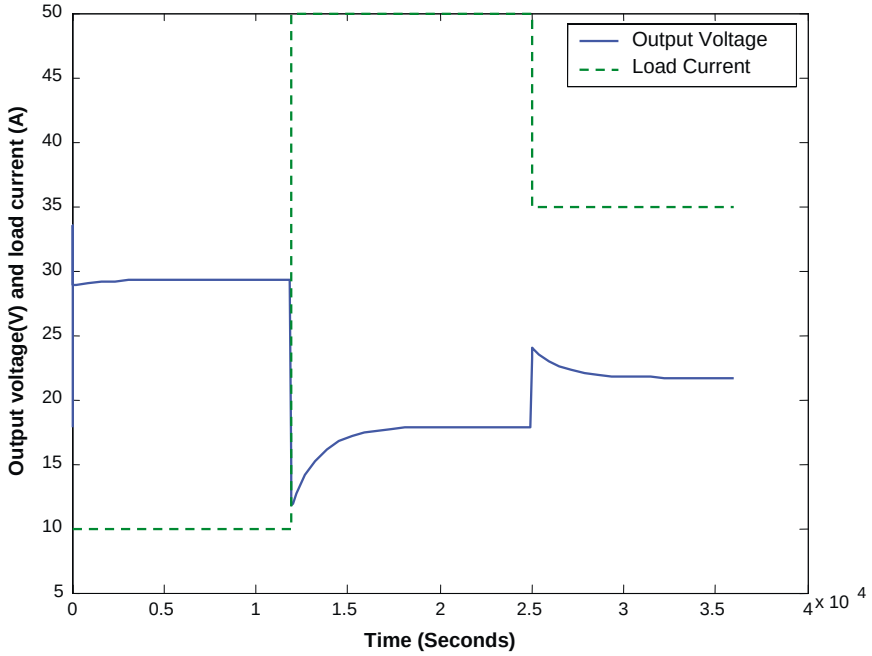

Fig. 5. Output voltage.

Table 2
Empirical MEA model coefficients

New model		Amphlett model [11]	
ξ_1	−0.97252	ξ_1	−0.9514
ξ_2	0.0034442	ξ_2	0.00312
ξ_3	9.3216E−005	ξ_3	7.4E−005
ξ_4	−0.00019141	ξ_4	−0.000187
ξ_5	0.016046	ξ_5	0.016046
ξ_6	−3.4715E−005	ξ_6	−3.4715E−005
ξ_7	7.9565E−005	ξ_7	7.9565E−005

modeling studies. In that approach, the effective surface partial pressure must be calculated based on the estimation of the pressure diffusivity product and the thickness of the gas diffuser portion of the electrode. The accurate estimation of these two parameters, however, is not straightforward. In this research we propose to simplify this procedure. When employing Fick's law, we use the gas partial pressure in the fuel cell channels to directly solve for the seven coefficients in the empirical relations. Using the data provided in [11], the model coefficients are obtained with a linear regression technique and are listed in Table 2. The coefficients of internal resistance model are the same as those given in [11], as the partial pressure has no effect on the internal resistance. While using the gas partial pressure in the Nernst equation could lead to certain errors, such errors can be compensated for in calculating the activation overvoltage. Fig. 4 shows the polarization curve comparison under the same conditions. The result obtained through the simplified approach shows good agreement with that given in [11].

3.3. Fuel cell dynamic model simulation

In this section, we carry out a detailed parametric analysis to study the transient dynamic effects within the fuel cell system. The parameters used in this part of study are listed in Table 3. For illustration purposes, the parameters we use are collected from the literature. Due to the unique improvement of the proposed model, certain parameters have not yet been considered by other studies and we then use those that could be representative of typical PEMFC systems. As some parameters such as lumped channel volumes are small, stiff differential equation solver ODE23S is employed in the simulation. The time length for the simulation is 36,000 s.

Fig. 5 shows the stack output voltage change corresponding to load current change. At 12,000 s, the current rises from 10 to 50 A, and the voltage drops from 29 to 18 V. At 25,000 s, the current goes down from 50 to 35 A, and the voltage goes up from 18 to 22 V. One can see that within each stage, while the respective current value remains constant, the voltage value keeps changing. The varying voltage is the result of combined effects due to the capacitance, time varying cell body temperature, and partial pressures of hydrogen and oxygen.

Fig. 6 shows the temperature histories of the stack body, anode channel and cathode channel. The temperatures of these three control volumes exhibit similar trends. During the first 12,000 s, the temperatures slowly increase. The reason is that the heat generated by the electrochemical reaction is more than the heat transferred to the surrounding atmosphere through convection. During the second stage (12,000–25,000 s), the output power of the stack increases due to the load current increase, and correspondingly the heat generated by the electrochemical reaction increases and overcomes the heat loss due to convection. Therefore, the temperatures of stack/anode/cathode all increase. During the last stage (25,000–36,000 s), the temperatures drop, as the output power and hence the heat generated is reduced. It is worth mentioning that the temperatures of the three control volumes differ significantly. This clearly demonstrates the advantage of dividing the fuel cell system into three control volumes.

Fig. 7 shows the pressure variation within the two channels. When the load current is high (50 A), the fuel consumed

Table 3
Parameters used in system simulation

Parameter	Value	Reference
$k_{up,an}$ (kg/(s atm))	3.6×10^{-6}	[a]
$k_{down,an}$ (kg/(s atm))	2.2×10^{-4}	[a]
$p_{s,an}$ (atm)	2.4	[12]
p_{atm} (atm)	1	Well known
$T_{an,in}$ (K)	296.5	[12]
$T_{an,out}$ (K)	296.5	[12]
c_{v,H_2} (J/(kg K))	10124.71	[19]
c_{p,H_2} (J/(kg K))	14209	[19]
M_{H_2} (kg/mol)	2.016	[19]
$k_{up,ca}$ (kg/(s atm))	3.6×10^{-4}	[a]
$k_{down,ca}$ (kg/(s atm))	2.2×10^{-3}	[a]
$p_{s,ca}$ (atm)	2.4	[12]
N	35	[12]
$T_{ca,in}$ (K)	296.5	[12]
$T_{ca,out}$ (K)	296.5	[12]
c_{v,O_2} (J/(kg K))	662.2	[19]
c_{p,O_2} (J/(kg K))	922	[19]
M_{O_2} (kg/mol)	32	[19]
c_{v,N_2} (J/(kg K))	745.2	[19]
c_{p,N_2} (J/(kg K))	1042	[19]
$k_{conv,amb}$ (W/K)	17	[12]
$k_{conv,an}$ (W/K)	2	[12]
$k_{conv,ca}$ (W/K)	10	[12]
$m_{body}c_{p,body}$ (J/K)	35000	[12]
F (A s/mol)	9.648456×10^4	[19]
$\Delta H_{R,T}$ (J)	1.196×10^8	Well known
Vol_{an} (m^3)	0.005	[13]
Vol_{ca} (m^3)	0.01	[13]
ξ_1	−0.9514	[11]
ξ_2	0.00312	[11]
ξ_3	−0.000187	[11]
ξ_4	7.4×10^{-5}	[11]
ξ_5	0.01605	[11]
ξ_6	-3.5×10^{-5}	[11]
ξ_7	8×10^{-5}	[11]
C (F)	2	[18]
T_{room} (K)	296.5	[12]

[a] These coefficients are so chosen that the maximum consumed fuel/gas is satisfied.

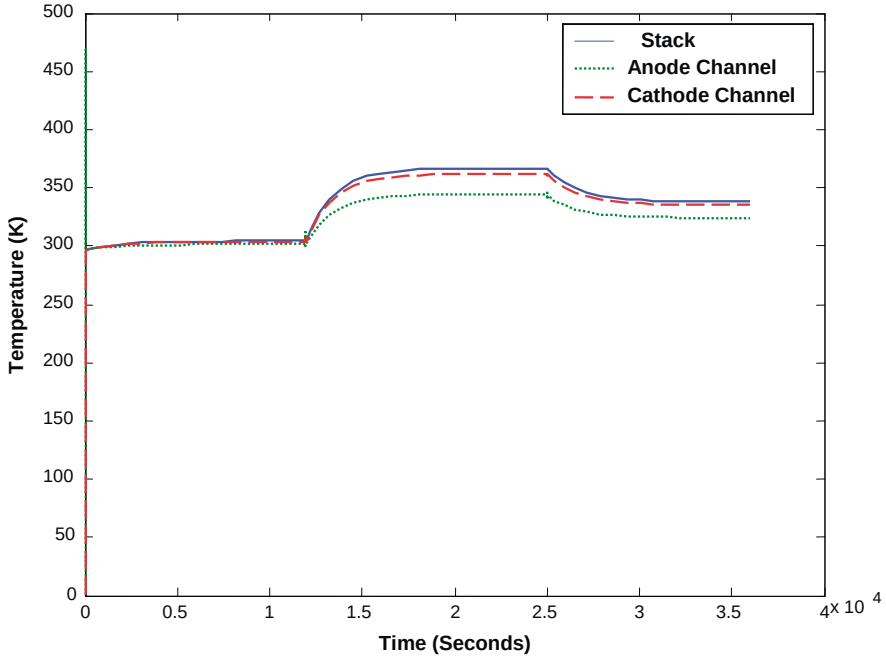

Fig. 6. Temperature history of stack/anode channel/cathode channel.

by the electrochemical reaction increases. Correspondingly, the gas pressures go down. On the contrary, when the load current is low (10, 35 A), the pressures within the channels become relatively high.

Figs. 8–10 show the change of mass of gases (hydrogen, oxygen and nitrogen) within the two channels due to the load current change. During the first stage and last stage, the load current is lower, which leads to lower fuel/oxygen consumption for the electrochemical reaction and higher mass of gases within the channels. The opposite can be observed for the second stage. It is shown that while hydrogen and oxygen decrease due to load current increase, the nitrogen mass goes up. This is because when the oxygen consumption increases, the pressure within the cathode channel goes down and more air will enter from the inlet, which causes the increase of nitrogen mass as nitrogen is not consumed by the electrochemical reaction. The inlet flow rates are shown in Figs. 11–13.

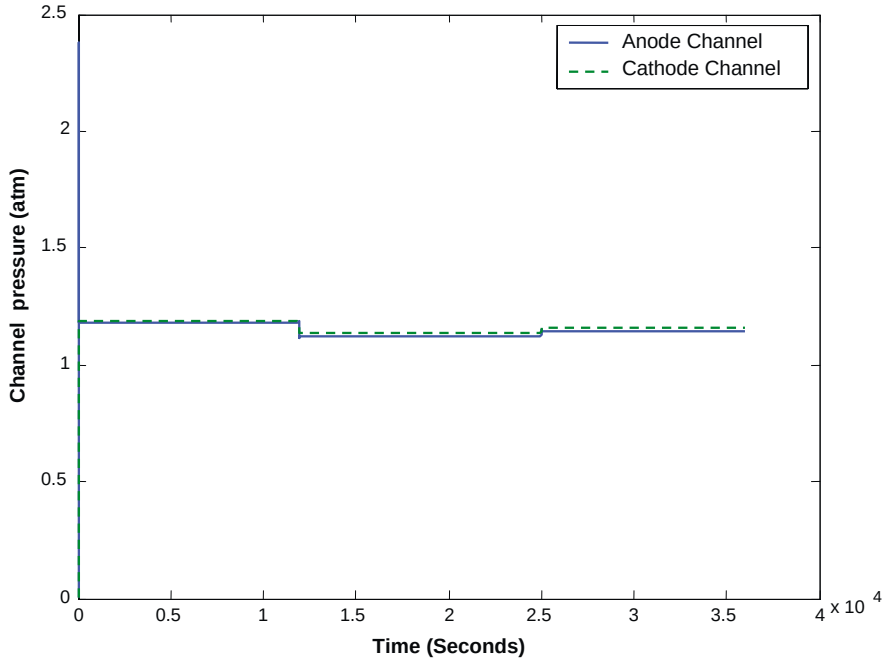

Fig. 7. Pressure changes within the anode and cathode channels.

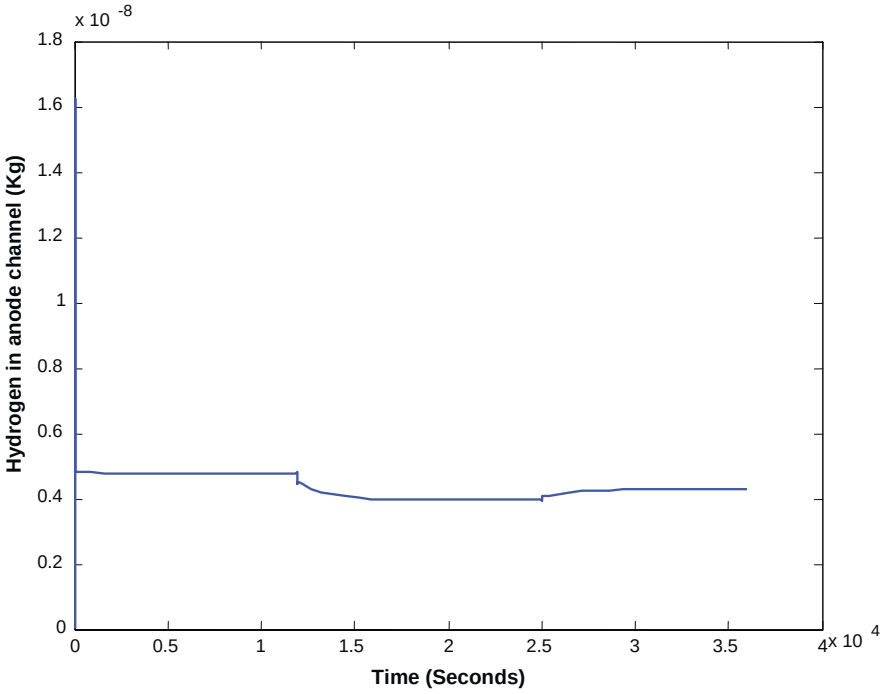

Fig. 8. Hydrogen change within anode channel.

The simulation results presented in this subsection clearly illustrates the complicated dynamic interactions between various components and effects (temperature, gas flow and capacitance, etc.), and demonstrates the necessity of developing a transient model using the control volume approach.

3.4. Experimental correlation and verification

To further validate the modeling strategy and provide more insight, a prototype fuel cell was designed for experimental test. The single cell consists of a Nafion membrane

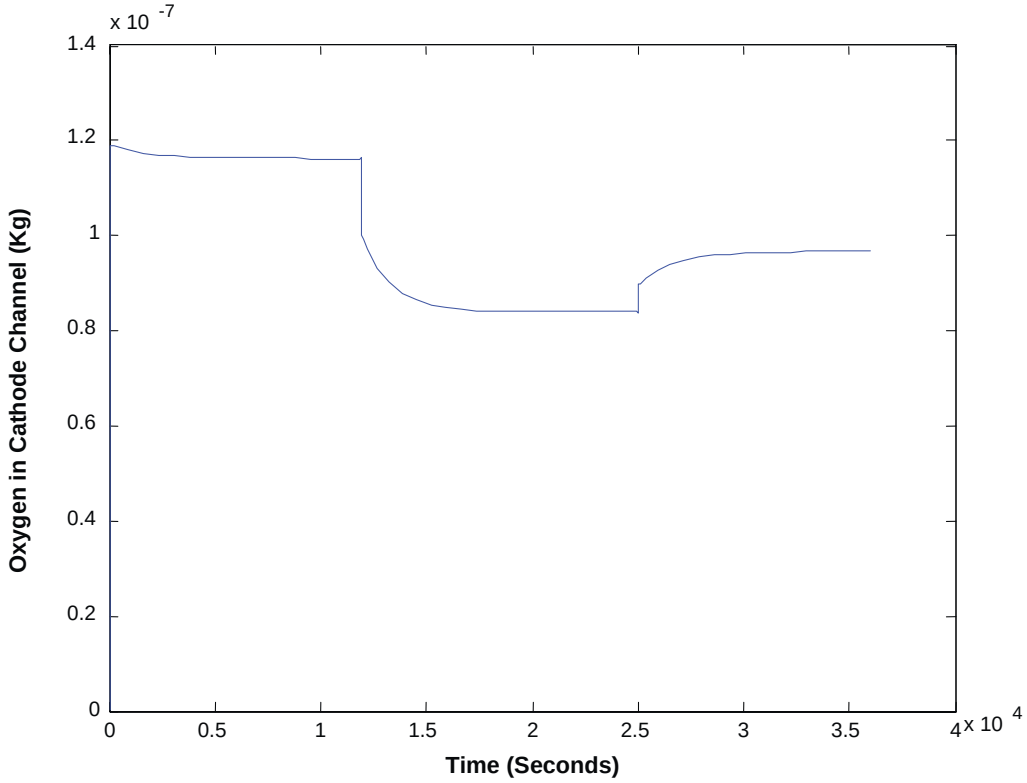

Fig. 9. Oxygen change within cathode channel.

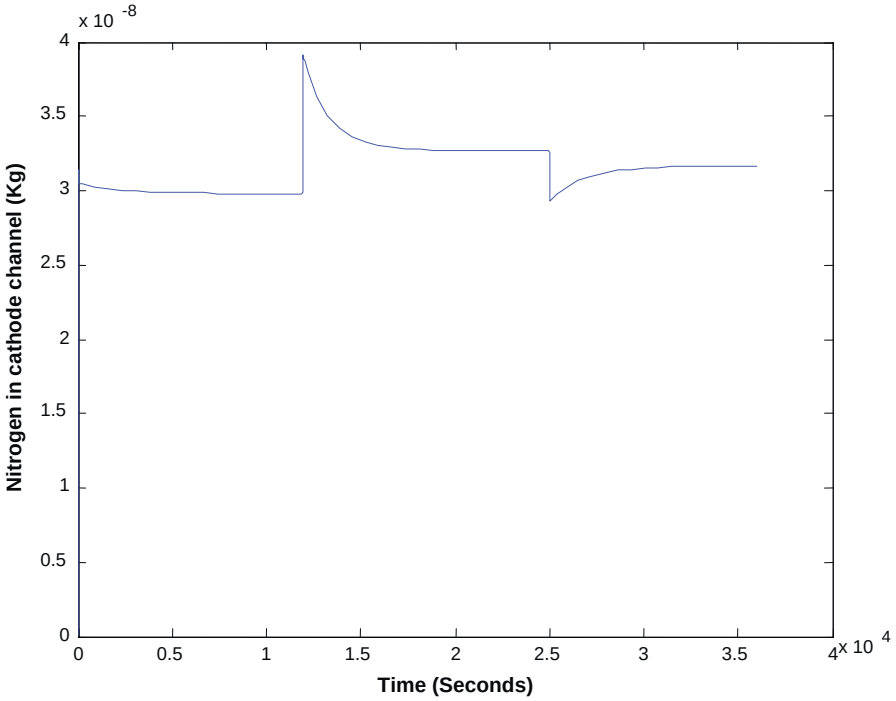

Fig. 10. Nitrogen change within cathode channel.

sandwiched between two carbon fiber paper electrodes. The surface area of the cell is 6.25 cm^2. In the experiment, pure hydrogen and oxygen are supplied to the anode and cathode channels. For experimental purpose, a temperature control unit is employed to introduce designated cell body temperature. A series of system input/output data (current, temperature, output voltage, ohmic overvoltage, inlet volume flow rates of anode and cathode channel) are recorded by the online measurement system. Three sets of experimental results are obtained.

For each set of experiment, we adjust the load current. Typically, the fuel cell operates for 300 s under one specified load current value, and the time interval between consecutive measurements is selected as 15 s. Therefore, 20 data points

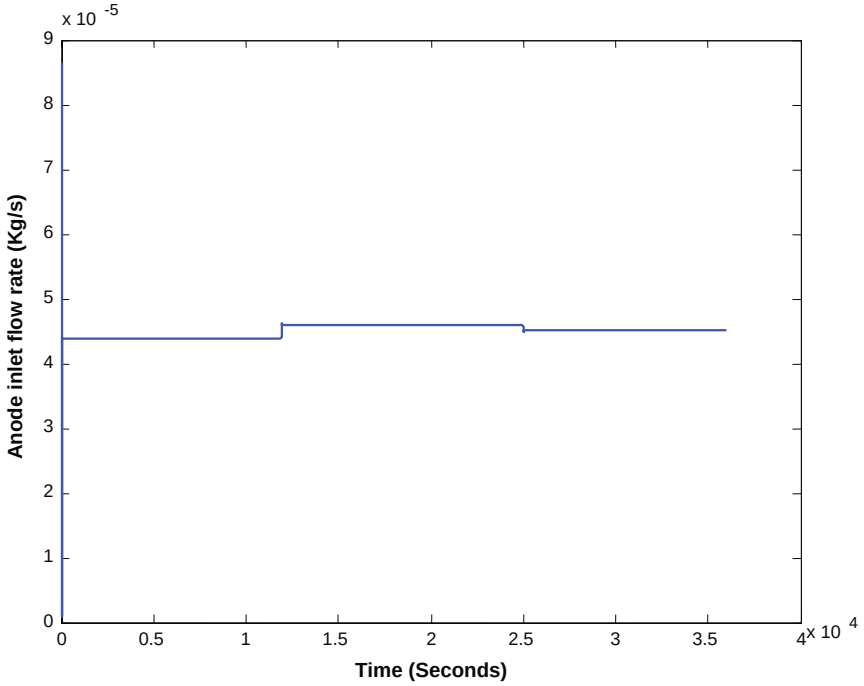

Fig. 11. Inlet flow rate of anode channel.

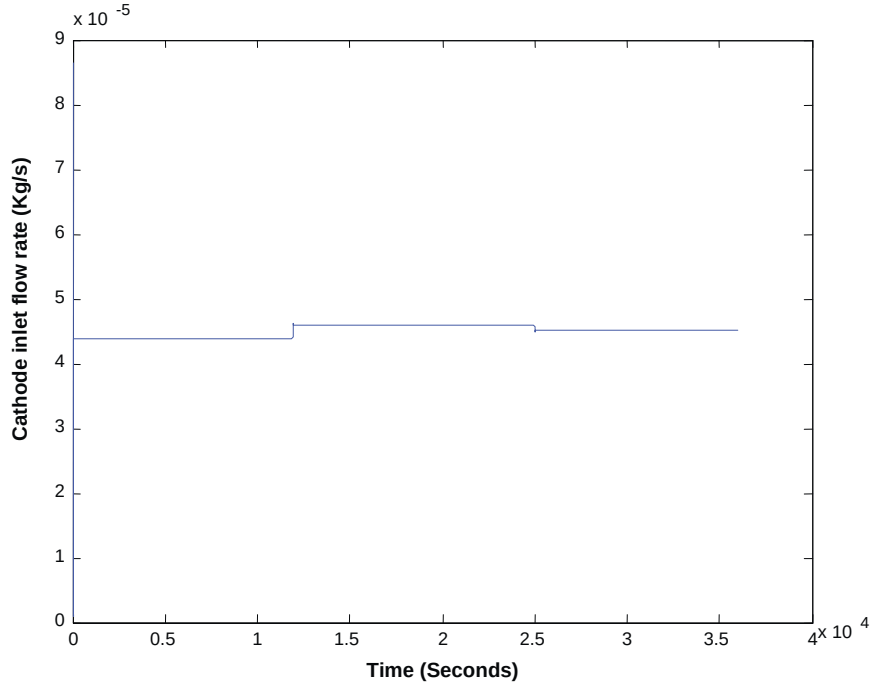

Fig. 12. Inlet oxygen flow rate of cathode channel.

can be obtained under one specific load current value. We measure the corresponding voltage output and other dependent variables such as inlet flow rate and ohmic overvoltage, and the results are listed in Table 4.

The volume flow rates listed in Table 4 can be converted into mass flow rates using the following equations [19]

$$p = \rho RT \tag{24}$$

$$\dot{m} = \rho \dot{V} \tag{25}$$

The mass flow rate coefficient given in Eq. (4) is a key parameter in exploring the dynamic behavior of the gases flowing through the channels. The upstream mass flow rate is estimated using the traditional nozzle equation [13]

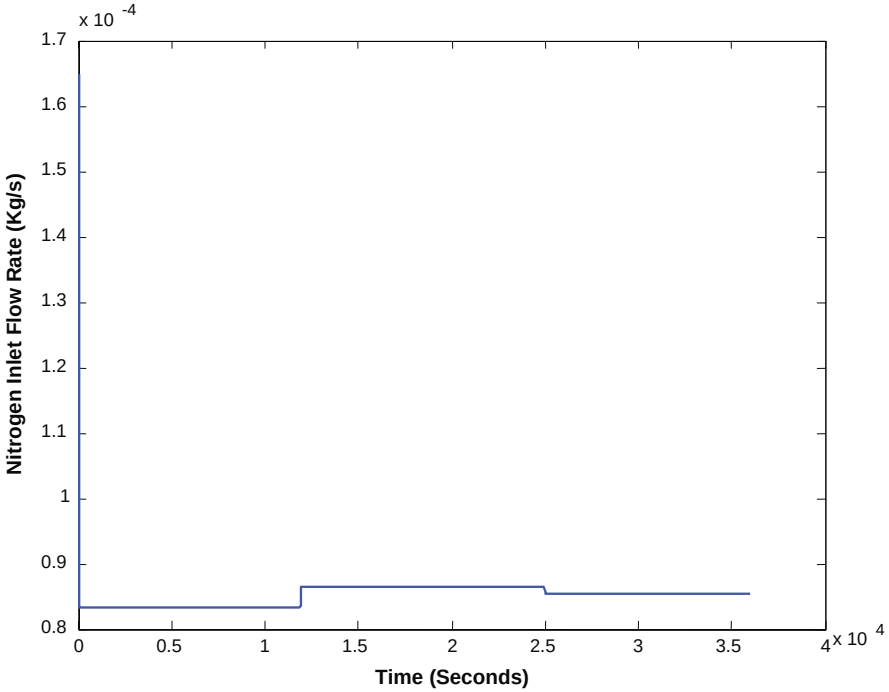

Fig. 13. Inlet nitrogen flow rate of cathode channel.

Table 4
Experimental data obtained from single cell test

T (K)	Current (A)	Total output voltage (V)	Ohmic overvoltage (V)	H_2 inlet flow rate (l/min)	O_2 inlet flow rate (l/min)
363	0.50003	0.77271	0.00971	0.20523	0.20188
363	1.00022	0.71458	0.03375	0.21075	0.20431
363	1.50024	0.6672	0.05078	0.21037	0.20704
363	1.99961	0.62471	0.06748	0.22179	0.2097
363	2.49986	0.58464	0.08467	0.22725	0.21266
363	2.99999	0.54541	0.10229	0.23278	0.2155
363	3.50002	0.50558	0.12056	0.23826	0.21813
363	3.9999	0.46499	0.139	0.24392	0.2207
363	4.49976	0.42315	0.15851	0.24924	0.22368
363	5.00031	0.37885	0.17983	0.25492	0.22638
363	5.50012	0.33093	0.20306	0.26036	0.22891
353	0.50001	0.81165	0.00492	0.20527	0.20155
353	1.00003	0.7755	0.01429	0.21086	0.20411
353	1.50007	0.75073	0.02147	0.2163	0.20705
353	2.00029	0.7283	0.02955	0.22178	0.20989
353	2.50014	0.70688	0.03761	0.22732	0.21246
353	2.99981	0.68706	0.04482	0.23286	0.21518
353	3.50002	0.67186	0.04766	0.23837	0.21799
353	4.00011	0.65476	0.05586	0.24384	0.22091
353	4.49992	0.63519	0.06545	0.24931	0.22353
353	5.00035	0.61905	0.07251	0.25478	0.22647
353	5.50008	0.60365	0.07991	0.26036	0.22882

$$k_{an,up} = 6.3 \times 10^{-12}\,\mathrm{kg/(s\,Pa)},$$
$$k_{ca,up} = 7.5979 \times 10^{-11}\,\mathrm{kg/(s\,Pa)}$$

Clearly, the outlet flow rate coefficient depends upon the pressure difference and temperature. Here, we treat the temperature as constant, as the temperature is indeed kept as constant in the experiment. An nth-order polynomial is used to interpolate the outlet flow coefficient

$$k_{down} = \sum_{i=1}^{n} c_i (\Delta P)^{n-i} \tag{26}$$

The coefficients in the above equation are obtained using the experimental results as shown in Table 5. After we obtain the mass flow rate coefficients, the pressures of hydrogen and oxygen in the channels can be solved using Eq. (1). Using the simplified method outlined in Section 3.2, the

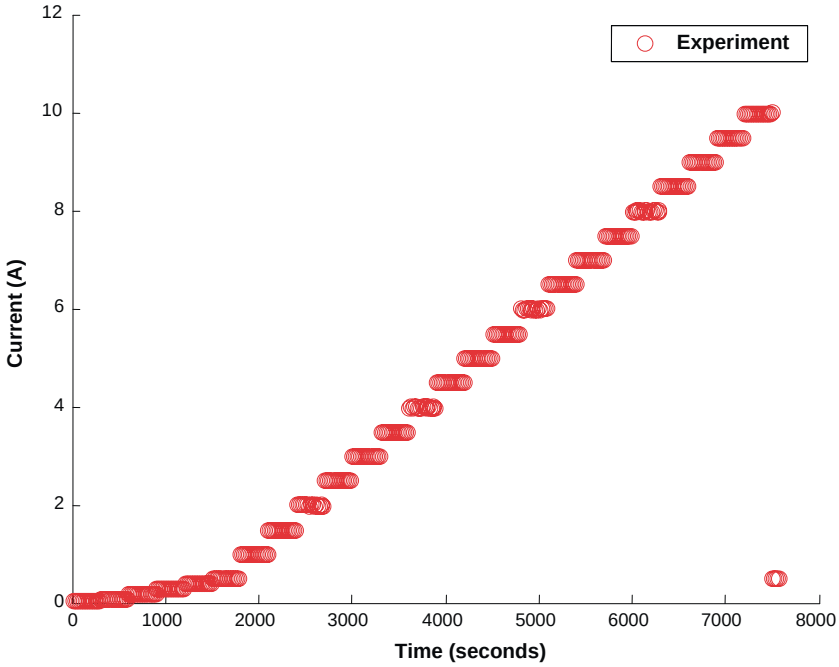

Fig. 14. Load current of experiment.

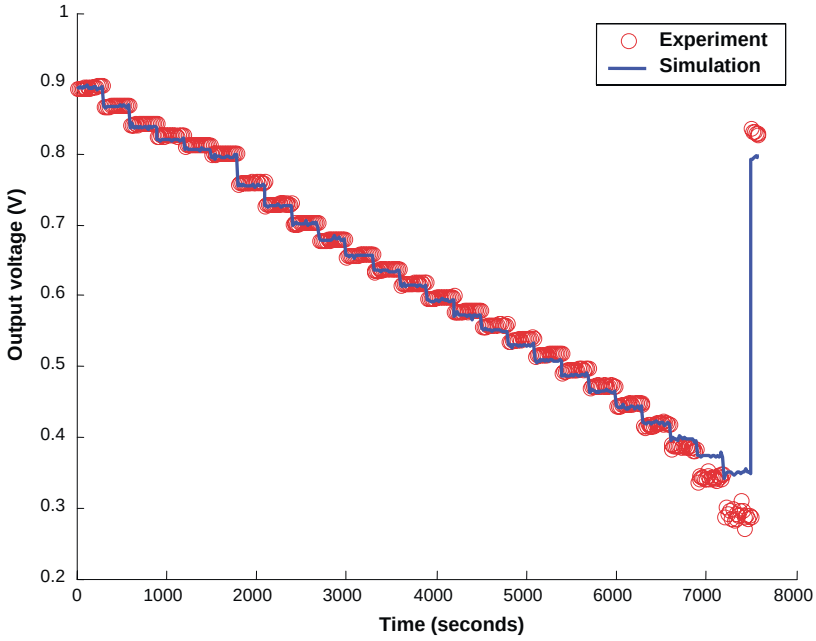

Fig. 15. Comparison of experimental and simulated output voltage.

Table 5
Outlet mass flow rate coefficients

Anode channel	Cathode channel
$c_1 = 4.7433\text{E}{-}030$	$c_1 = -2.084\text{E}{-}034$
$c_2 = -1.0812\text{E}{-}024$	$c_2 = 9.1435\text{E}{-}029$
$c_3 = 9.7248\text{E}{-}020$	$c_3 = -1.6348\text{E}{-}023$
$c_4 = -4.3164\text{E}{-}015$	$c_4 = 1.5164\text{E}{-}018$
$c_5 = 9.0445\text{E}{-}011$	$c_5 = -7.6298\text{E}{-}014$
	$c_6 = 1.886\text{E}{-}009$

Table 6
Coefficients associated with MEA model

Coefficients in Eq. (15)	Coefficients in Eq. (17)
$\xi_1 = 0.581$	$\xi_5 = -0.133$
$\xi_2 = 0.02536$	$\xi_6 = 4.103 \times 10^{-4}$
$\xi_3 = 1.044 \times 10^{-4}$	$\xi_7 = 7.9584 \times 10^{-4}$
$\xi_4 = -1.0028 \times 10^{-3}$	

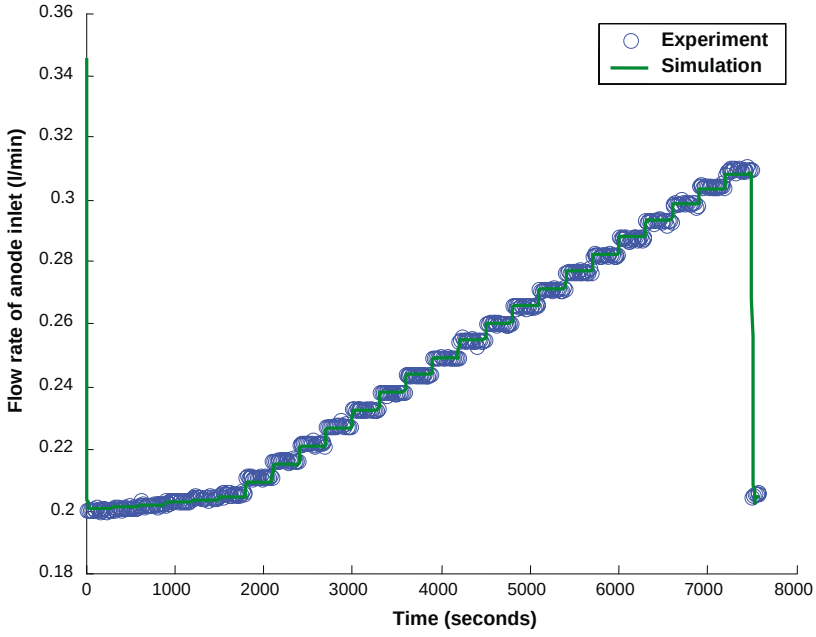

Fig. 16. Comparison of experimental and simulated anode inlet flow rate.

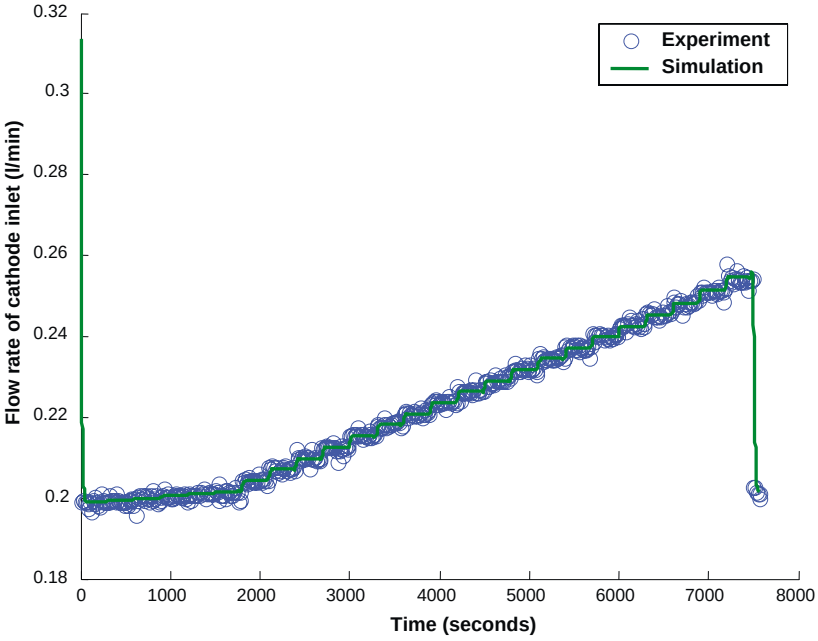

Fig. 17. Comparison of experimental and simulated cathode inlet flow rate.

coefficients related to activation overvoltage and internal resistances can be solved using a linear regression technique, which are shown in Table 6. Two sets of experimental data are used for identifying the key parameters used in the dynamic model, and the other set is used to compare between the simulation and experimental investigation. The load current history is shown in Fig. 14. To facilitate the simulation, the experiment data are interpolated into continuous current signal with a third-order spline function. Here the current is used as the input signal to the dynamic model, and the output voltage and inlet flow rates of anode and cathode channels are simulated.

Fig. 15 shows a comparison between experimental and simulated output voltage. In general, the simulation results exhibit excellent agreement with actual cell performance. At very large current values, one can observe certain deviation between the predicted and experimental voltage values. One reason is that a very large current will cause a large number of water molecules be dragged by the hydrogen proton from anode side to cathode side, which could lead to the flooding of the cathode catalyst and membrane drying at anode side. Both effects could actually deteriorate the performance of the cell [1–7]. Another possible reason is the cell temperature effect. Only two cell temperature values are used in the experiment, 80 and 90 °C. These two temperature values might not be enough to cover the entire operating range.

Figs. 16 and 17 show the comparison between the experimental and simulated inlet flow rates at anode and cathode channels. Again, one can see excellent agreement between model prediction and experimental result.

4. Conclusion

In this study, we have developed a system-level dynamic model of PEMFC that incorporates the complicated temperature, gas flow through the channel and the capacitance formed by double charged layer of MEA under operating conditions. To clearly quantify the dynamic interactions, we divide the fuel cell system into three control volumes, the anode channel, the cathode channel, and the fuel cell body, and develop respective lumped-parameter dynamic models. The system-level model is simulated using SIMULINK. Extensive numerical studies are carried out and it has been demonstrated that the developed model can capture the transient dynamic behavior of the fuel cell system. We have also performed an experimental study and have illustrated excellent agreement between the predicted and experimental results.

Acknowledgements

Support for this fuel-cell related research was supplied by the US Army (Advanced Technology for Portable Miniature and Micro Fuel Cells, US ARMY CECOM, Agreement No. DAAB07-03-3-K-415) and by the Connecticut Global Fuel Cell Center.

References

[1] P. Costamagna, S. Srinivasan, Quantum jumps in the PEMFC science and technology from the 1960s to the year 2000. Part II. Engineering,

technology development and applications aspects, J. Power Sources 102 (2001) 253–269.
[2] D.M. Bernardi, M.W. Verbrugge, Mathematical model of a gas diffusion electrode bonded to a polymer electrolyte, AIChE J. 37 (8) (1991) 1151–1163.
[3] D.M. Bernardi, M.W. Verbrugge, A mathematical model of the solid polymer electrolyte fuel cell, J. Electrochem. Soc. 139 (9) (1992) 2477–2491.
[4] T.E. Springer, M.S. Wilson, S. Gottesfeld, Modeling and experimental diagnostics in polymer electrolyte fuel cells, J. Electrochem. Soc. 140 (12) (1993) 3513–3526.
[5] A. Rowe, X. Li, Mathematical modeling of proton exchange membrane fuel cells, J. Power Sources 102 (2001) 82–96.
[6] M. Wohr, K. Bolwin, W. Schnurnberger, M. Fischer, W. Neubrand, G. Eigenberger, Dynamic modeling and simulation of a polymer membrane fuel cell including mass transport limitation, Int. J. Hydrogen Energy 23 (3) (1998) 213–218.
[7] M. Ceraolo, C. Miulli, A. Pozio, Modeling static and dynamic behavior of proton exchange membrane fuel cell on the basis of electrochemical description, J. Power Sources 113 (2003) 131–144.
[8] H. Ide, T. Yoshida, H. Ueda, H. Horiuchi, Natural gas reformed fuel cell power generation systems—a comparison of three system efficiencies, in: Proceedings of the 24th Intersociety Energy Conversion Engineering Conference, vol. 3, Washington, DC, USA, 1989, pp. 1517–1522.
[9] J.C. Amphlett, R.M. Baumert, R.F. Mann, B.A. Peppley, P.R. Roberge, A. Rodrigues, Parametric modeling of the performance of a 5-kW proton-exchange membrane fuel cell stack, J. Power Sources 49 (1994) 349–356.
[10] J.C. Amphlett, R.M. Baumert, R.F. Mann, B.A. Peppley, P.R. Roberge, T.J. Harris, Performance modeling of the Ballard Mark IV solid polymer electrolyte fuel cell. I. Mechanistic model development, J. Electrochem. Soc. 142 (1) (1995) 1–9.
[11] J.C. Amphlett, R.M. Baumert, R.F. Mann, B.A. Peppley, P.R. Roberge, T.J. Harris, Performance modeling of the Ballard Mark IV solid polymer electrolyte fuel cell. II. Empirical model development, J. Electrochem. Soc. 142 (1) (1995) 10–15.
[12] J.C. Amphlett, R.F. Mann, B.A. Peppley, P.R. Roberge, A. Rodrigues, A model predicting transient responses of proton exchange membrane fuel cells, J. Power Sources 61 (1–2) (1996) 183–188.
[13] J.T. Pukrushpan, H. Peng, A.G. Stefanopoulou, Simulation and analysis of transient fuel cell system performance based on a dynamic reactant flow model, Proceedings of ASME IMECE, New Orleans, Louisiana, USA, 2002.
[14] M.T. Iqbal, Modeling and control of a wind fuel cell hybrid energy system, Renewable Energy 28 (2003) 223–237.
[15] S. Yerramalla, A. Davari, A. Feliachi, T. Biswas, Modeling and simulation of the dynamic behavior of a polymer electrolyte membrane fuel cell, J. Power Sources 124 (2003) 104–113.
[16] F.M. White, Viscous Fluid Flow, second ed., McGraw-Hill, 1991.
[17] R.F. Mann, J.C. Amphlett, A.I. Hooper, H.M. Jensen, B.A. Peppley, P.R. Roberge, Development and application of a generalized steady-state electrochemical model for a PEM fuel cell, J. Power Sources 86 (2000) 173–180.
[18] J. Larminie, A. Dicks, Fuel Cell Systems Explained, Wiley, 2000.
[19] R.E. Sonntag, C. Borgnakke, G.J. Van Wylen, Fundamentals of Thermodynamics, sixth ed., Wiley, 2003.